Global and Planetary Change 204 (2021) 103584

Contents lists available at ScienceDirect

Global and Planetary Change

journal homepage: www.elsevier.com/locate/gloplacha

Cyclostratigraphy of the Cryogenian Fiq Formation, Oman and its implications for the age of the Marinoan glaciation

Zheng Gong *

Department of Earth and Planetary Sciences, Yale University, New Haven, CT, USA

ARTICLE INFO

Editor: Dr. Maoyan Zhu

Keywords:
Cryogenian
Marinoan glaciation
Snowball Earth
Cyclostratigraphy
Fiq Formation
Oman

ABSTRACT

Cyclostratigraphy is a powerful tool in chronostratigraphic studies, and has shown its potential in Precambrian time. The Cryogenian Period is one of the most dynamic and intriguing intervals in Earth history and it is a witness to the most extreme climate changes on the planet, known as two Snowball Earth events. However, a robust chronostratigraphic framework is still lacking especially for the younger Marinoan Snowball Earth event, hampering the stratigraphic correlation and comparison among geographically separated records, as well as the understanding of the initiation and termination of this global-scale glaciation. The Cryogenian Fiq Formation in Oman is thought to be Marinoan-equivalent. The duration of the nonglacial units in the Fiq Formation could provide a conservative age constraint on the previously not well-determined onset age of the Marinoan glaciation. In this work, a cyclostratigraphic study has been conducted on three drill cores of the Fiq Formation. The multi-taper method (MTM) spectral analysis, the correlation coefficient (COCO), and the evolutionary correlation coefficient (eCOCO) analyses were performed on the high-resolution gamma-ray (GR) data from the three cores. A hierarchy of Milankovitch cycles (eccentricities, obliquities, and precessions) has been identified, which was used to estimate the optimal sedimentary accumulate rates and the duration of the Fiq Formation in each core. Based on the cyclostratigraphic results, the time scale of the Fiq Formation is at least ~6 Myr. Integrating the radiometric ages and the cyclostratigraphic data from other continents, the onset age of the Marinoan glaciation is suggested to be 650–641 Ma. This new result helps improve the chronostratigraphic framework for the Cryogenian Period and also provides critical temporal constraints for the geological and numerical models that explore the possible mechanisms for the Snowball Earth events.

1. Introduction

Stratigraphic correlation and calibration in Precambrian time are difficult due to the rarity of absolute ages from radiometric dating and the lack of a cosmopolitan biostratigraphy. Using chemostratigraphy for correlation such as the commonly used $\delta^{13}C$ profile often requires the assumption that the isotopic values are globally representative, which is not always the case (Cramer and Jarvis, 2020). Alternatively, cyclostratigraphy is a useful tool to calibrate time in the Precambrian. Cyclostratigraphy detects astronomically-forced climate cycles (i.e. Milankovitch cycles) that are encoded as lithological variations in the sequences of sedimentary rocks (Hinnov, 2013, 2018; Kodama and Hinnov, 2014). It could be utilized to estimate the sedimentation rates of the strata, the duration of the geological events, and when combined with radiometric ages, it could provide extrapolated age constraints as well. Applications of cyclostratigraphy can be traced back to Neoarchean-Paleoproterozoic Eons to explore the potential astronomical forcing on the deposition of banded iron formations (Lantink et al., 2019; Rodrigues et al., 2019). Continuous operation of the Milankovitch cycles has been observed globally in Mesoproterozoic (Mei and Tucker, 2013; Zhang et al., 2015; Cheng et al., 2020; Lyu et al., 2021; Mitchell et al., 2021a) and Neoproterozoic successions (Minguez et al., 2015; Fairchild et al., 2016; Minguez and Kodama, 2017; Gong et al., 2017, 2019; Bao et al., 2018; Sui et al., 2018, 2019; Gong and Li, 2020; Mitchell et al., 2021b). These studies demonstrate the power of cyclostratigraphy in chronostratigraphic studies in Precambrian time.

Cyclostratigraphic studies in the Cryogenian are scarce, despite the fact that a robust chronostratigraphic framework is of great importance during this period. The Cryogenian Period (ca. 720–635 Ma, Shields-Zhou et al., 2016) marks one of the coldest time intervals in Earth history. It is suggested that two Snowball Earth events (namely the Sturtian and Marinoan glaciations) occurred during the Cryogenian when

* Corresponding author.
E-mail address: z.gong@yale.edu.

https://doi.org/10.1016/j.gloplacha.2021.103584
Received 16 February 2021; Received in revised form 17 May 2021; Accepted 19 July 2021
Available online 24 July 2021

glaciers advanced to equatorial regions (Fig. 1A; Kirschvink, 1992; Hoffman et al., 1998, 2017). Whether the global ocean was entirely frozen ("hard" Snowball Earth) or there existed open waters in the tropics ("soft" Snowball Earth) is still a matter of debate, and both scenarios could be defended in geological or climate modeling perspectives (Leather et al., 2002; Lewis et al., 2007; Allen and Etienne, 2008; Yang et al., 2012; Hoffman et al., 2017). However, the positive ice-albedo feedback would promote a fast glaciation process and require the initiation of the Snowball Earth events to be global synchronous, regardless of "hard" or "soft" scenarios. In the last two decades, precise absolute ages have been obtained from the Sturtian and Marinoan records worldwide using the U-Pb geochronology on zircons from ash beds and the Re-Os geochronology on rocks enriched in organic matters. These ages suggest that the onset and termination ages of the Sturtian glaciation are ~717 Ma and ~660 Ma, and the termination age of the Marinoan glaciation is ~635 Ma (Fig. 1B; reviewed in Hoffman et al., 2017). Yet, the onset age of the Marinoan glaciation is uncertain, ranging widely from 657 Ma to 639 Ma (Fig. 1B; Kendall et al., 2006; Zhang et al., 2008; Lan et al., 2015; Prave et al., 2016; Bao et al., 2018; Nelson et al., 2020; Rooney et al., 2020). Among these attempts, cyclostratigraphy has been utilized to determine the onset age of the Marinoan glaciation. Bao et al. (2018) studied the interglacial Datangpo Formation in South China, and estimated that the two Snowball Earth events were temporally separated by ~10 million years. Based on the termination age of the Sturtian glaciation, Bao et al. (2018) suggested that the Marinoan glaciation began at ~650 Ma, which falls within the onset age range of the Marinoan glaciation that is constrained by radiometric ages from South China, Congo, and Laurentia (Fig. 1B; Zhang et al., 2008; Lan et al., 2015; Prave et al., 2016; Nelson et al., 2020; Rooney et al., 2020). However, a Re-Os age from South Australia suggests that the Marinoan glaciation should be younger than 643.0 ± 2.4 Ma (Kendall et al., 2006) although the reliability of this age is challenged by Rooney et al. (2014). Thus, more age constraints are still needed from different Marinoan records in order to better constrain its onset age.

This study focused on the Cryogenian Fiq Formation in Oman, which is regarded as an equivalent succession to the Marinoan glaciation (Allen, 2007). The Fig Formation is characterized by repeated diamictites interbedded with nonglacial siliciclastic units (Allen et al., 2011). Cyclostratigraphic analysis on the nonglacial units could directly provide a conservative duration for the Fiq Formation, which could be useful to constrain the onset age of the Marinoan glaciation.

2. Geological background

In Neoproterozoic time, Oman was located in the tropics with a paleolatitude of ~10–15° (Fig. 1A; Kempf et al., 2000; Kilner et al., 2005). Oman provides a suite of kilometer-thick Cryogenian strata that overlie the ca. 850–800 Ma crystalline basement (Fig. 2B; Gorin et al., 1982; Allen, 2007; Bowring et al., 2007). Nonconformably above the basement rocks is the Cryogenian Abu Mahara Group, which, in ascending order, consists of the glaciogenic Ghubrah Formation, a cap carbonate layer, the siliciclastic Arkahawl and Marsham Formations, a volcaniclastic Saqlah Member, and the glaciogenic Fiq Formation. The Ghubrah Formation is dated to be ~713 Ma by the U-Pb thermal ionization mass spectrometry (TIMS) geochronology on zircons from a tuffaceous sandstone and is believed to be time-correlative to the Sturtian glaciation (Fig. 2B; Bowring et al., 2007). The cap carbonates sitting directly above the Ghubrah Formation is commonly observed in global Sturtian records (Hoffman et al., 2017). The Arkahawl and Marsham Formations represent the interglacial period between the two Snowball Earth events, which is overlain by the Saqlah volcanics (Fig. 2B; Allen et al., 2011). The Fiq Formation has no absolute age constraint, but detrital zircon geochronology indicates that the maximum depositional age of the uppermost part of this formation is ~645 Ma (Bowring et al., 2007). The Fiq Formation, consisting of alternative diamictite siliciclastic layers, was deposited in a rift environment and is suggested as a record of the Marinoan glaciation (Allen, 2007; Bowring et al., 2007). The repeated glacial-interglacial transitions preserved in the Fiq Formation are considered to support a "soft" Snowball Earth scenario

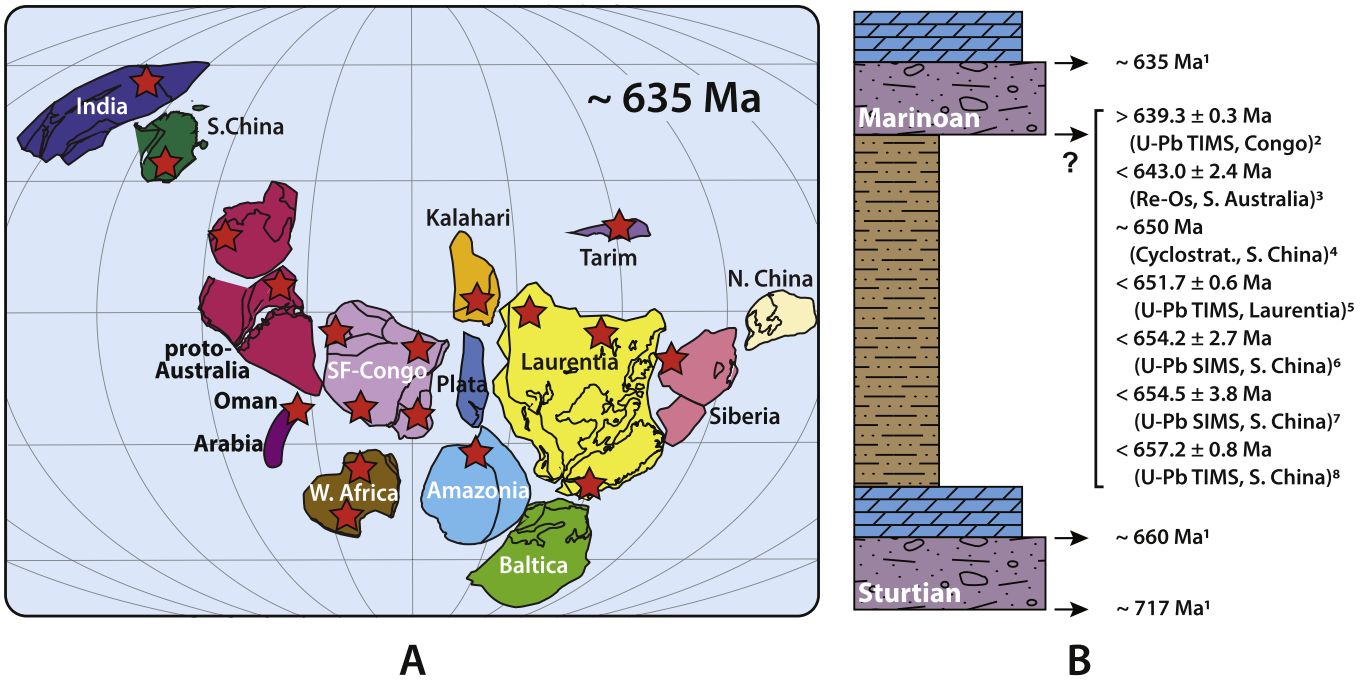

Fig. 1. Paleogeographic reconstruction model is from Zhang et al. (2013) and Bao et al. (2018). The red stars represent the records of Marinoan glaciation compiled by Hoffman et al. (2017). (B) Available age constraints on the Cryogenian Snowball Earth events. Geochronological references: 1. Hoffman et al. (2017); 2. Prave et al. (2016); 3. Kendall et al. (2006); 4. Bao et al. (2018); 5. Nelson et al. (2020); 6. Lan et al. (2015); 7. Zhang et al. (2008); 8. Rooney et al. (2020). (For interpretation of the references to colour in this figure legend, the reader is referred to the web version of this article.)

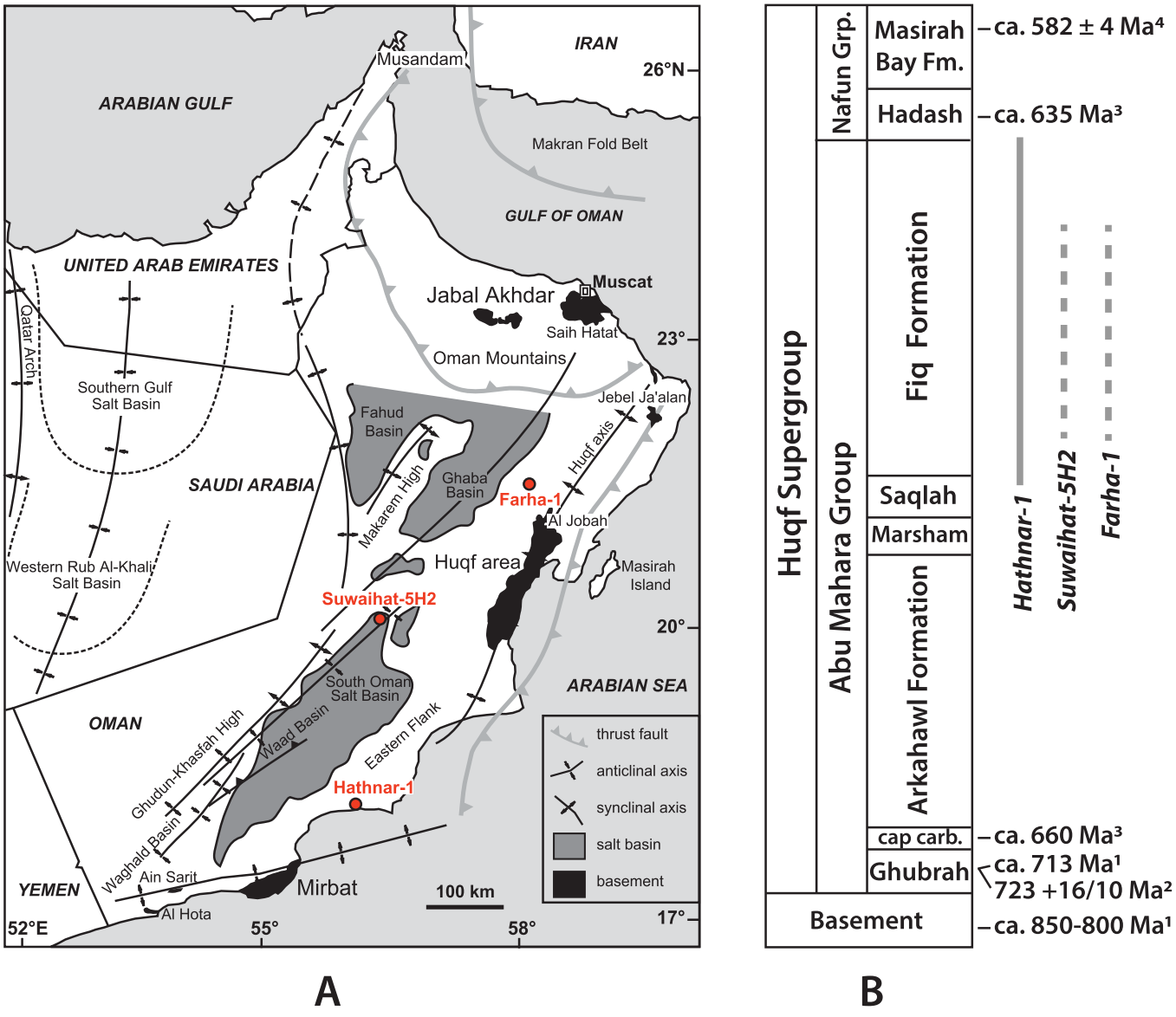

Fig. 2. (A) Geologic map of Oman (modified from Allen et al., 2011). The black regions are exposures of the Neoproterozoic strata. The grey regions are salt basins. The red dots show the locations of the three drill cores of this study. (B) Simplified stratigraphy of the Abu Mahara Group. Geochronological references: 1. Bowring et al. (2007); 2. Brasier et al. (2000); 3. Correlation by cap carbonates; 4. Cantine et al. (2019). Stratigraphic positions of three drill cores are marked with vertical lines. Grey vertical solid and dashed lines represent the stratigraphic coverage of three cores. The positions of the Suwaihat-5H2 and Farha-1 cores are not certain but should be closer to the lower part of the Fiq Formation given the absence of diamictites, therefore represented by dashed lines. Formation thicknesses are not to scale. Grp. = Group, Fm. = Formation, carb. = carbonates. (For interpretation of the references to colour in this figure legend, the reader is referred to the web version of this article.)

(Leather et al., 2002; Rieu et al., 2007; Allen and Etienne, 2008). The Fiq Formation is immediately overlain by the Hadash cap carbonates which are dolomitic and characterized by negative carbon isotopic values (Leather et al., 2002; Allen et al., 2011). Sharing many common features of the worldwide Marinoan cap carbonates, the Hadash cap carbonates are correlated to be ~635 Ma (Fig. 2B; Condon et al., 2005; Allen et al., 2011).

3. Materials and methods

The three sections of the Fiq Formation in this study are drill cores from different areas of Oman (Fig. 2A). For instance, the Hathnar-1 core (GPS: 18.04°N, 56.03°E) is along the southern coast near the southeast margin of the South Oman Salt Basin, the Suwaihat-5H2 core (20.01°N, 56.32°E) is located at the northernmost South Oman Salt Basin, while the Farha-1 core (21.47°N, 58.02°E) is between the Ghaba Basin and the Huqf area (Fig. 2A). These areas are far from the recently uplifted and structurally complicated Oman Mountains in the northeast (Fig. 2A; Hansman et al., 2017). Outcrops of the Neoproterozoic strata in Mirbat and Huqf areas show gentle tilting, with an average of ~20° (Kempf et al., 2000; Kilner et al., 2005). These three cores were drilled by the Petroleum Development Oman (PDO) company. The lithology was described in detail and the gamma-ray (GR) logging was employed with a sub-meter resolution (Fig. 3). These data are reported in Forbes et al. (2010). Raw GR data are available in Table S1. GR value is a measure of natural radioactivity, which is mainly emitted from minerals that are enriched in potassium (K), thorium (Th), uranium (U), etc. For example, igneous units are commonly characterized by high GR values. GR values of clay-rich beds are usually higher than carbonate-rich beds. Thus, GR values are strongly correlated with the lithology, and the changes of GR

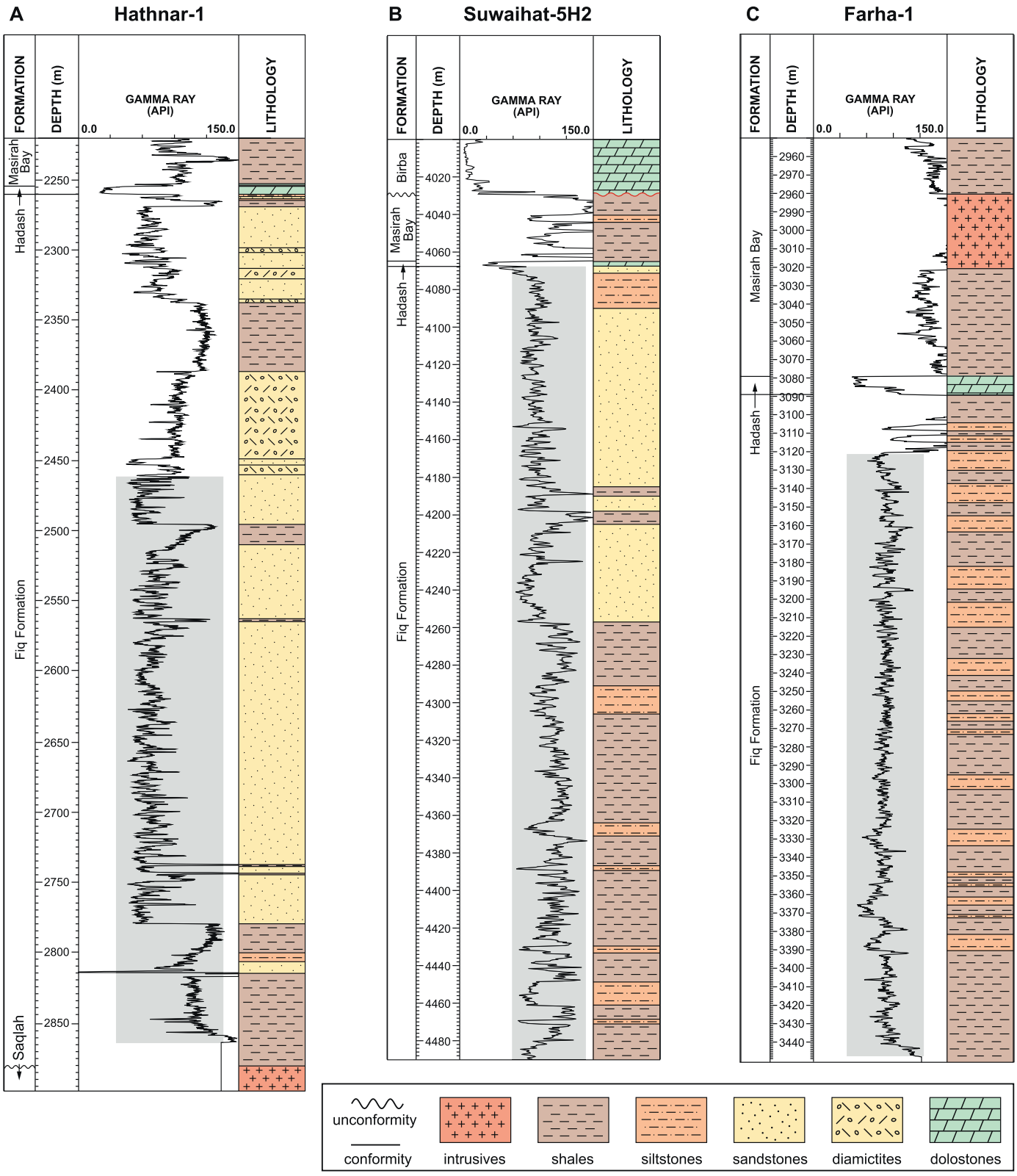

Fig. 3. Stratigraphic columns and raw GR series of the (A) Hathnar-1 core, (B) Suwaihat-5H2 core, and (C) Farha-1 core (modified from Forbes et al., 2010). The shaded grey boxes show the GR data that are included in time-series analyses. (For interpretation of the references to colour in this figure legend, the reader is referred to the web version of this article.)

values could be used as a proxy to reflect the lithological variations that are controlled by astronomical forcing (Li et al., 2019a; Gong and Li, 2020).

The Hathnar-1 core starts with the Saqlah Member at the bottom, which is composed of amygdaloidal and microcrystalline basalts (Fig. 3A; Forbes et al., 2010). Overlying the Saqlah Member is a ~400 m thick siliciclastic unit of the Fiq Formation (Fig. 3A). In general, GR values are high in shaly and silty layers and low in sandy layers (Fig. 3A).

Between 2470 m and 2270 m, several diamictite units are interbedded with the siliciclastic units, which are interpreted to represent local glacial-interglacial transitions near Oman (Allen et al., 2011). The matrix of the diamictites has a chloritic composition with various exotic clasts (Fig. S1; Forbes et al., 2010). The Fiq Formation is terminated with the 10-m Hadash cap carbonates overlain on top. The decrease of GR values also points to the sharp lithological transition from the siliciclastic rocks in the Fiq Formation to the carbonate rocks in the Hadash Formation (Fig. 3A). The Fiq Formation in the Suwaihat-5H2 core is ~420 m in thickness, which is dominated by shales and siltstones in the lower part and sandstones in the upper part (Fig. 3B). No diamictites are observed in this core. The ~10-m Hadash cap carbonates lie on top of the Fiq Formation in the Suwaihat-5H2 core (Fig. 3B). In the Farha-1 core, the thickness of the Fiq Formation is about 320 m, which consists of the interbedded shales and siltstones (Fig. 3C). The diamictites are not identified in this core. The upper boundary of the Fiq Formation is defined by a 10-m Hadash cap carbonate layer as well (Fig. 3C). No obvious depositional hiatus was identified from the three cores. However, these cores are likely affected by glacial erosion below the Hadash Formation, which is particularly for the Suwaihat-5H2 and Farha-1 cores due to the absence of diamictite layers (Fig. 3). Also, drilling did not penetrate to the Saqlah Member in the Suwaihat-5H2 and Farha-1 cores (Fig. 3), indicating that the Fiq Formation was not completely sampled there. The stratigraphic correlation among the three cores is not straightforward, given that the Fiq Formation was deposited in a rift basin (Allen, 2007). Therefore, the lithology is strongly controlled by local environments and exhibits significant lateral heterogeneity (Allen, 2007). It is tentatively proposed that the shale-siltstone unit from 4490 m to 4260 m segment of the Suwaihat-5H2 core possibly matches the 3450–3120 m shale-siltstone unit of the Farha-1 core (Fig. 3), considering their thickness and lithology. The 2770–2460 m sandstone unit of the Hathnar-1 core could be correlated to the 4260–4090 m sandstone unit of the Suwaihat-5H2 core (Fig. 3). Nonetheless, the top layers of the three cores are undoubtedly correlated by the Hadash cap carbonates (Fig. 3).

This study only included the GR data from the nonglacial siliciclastic units of the Fiq Formation, while the data from the diamictite and igneous units were subtracted from the series (Fig. 3; Table S1). Data included are shown with the shaded grey boxes in Fig. 3. This treatment would lead to an underestimate of the duration of the Fiq Formation. For

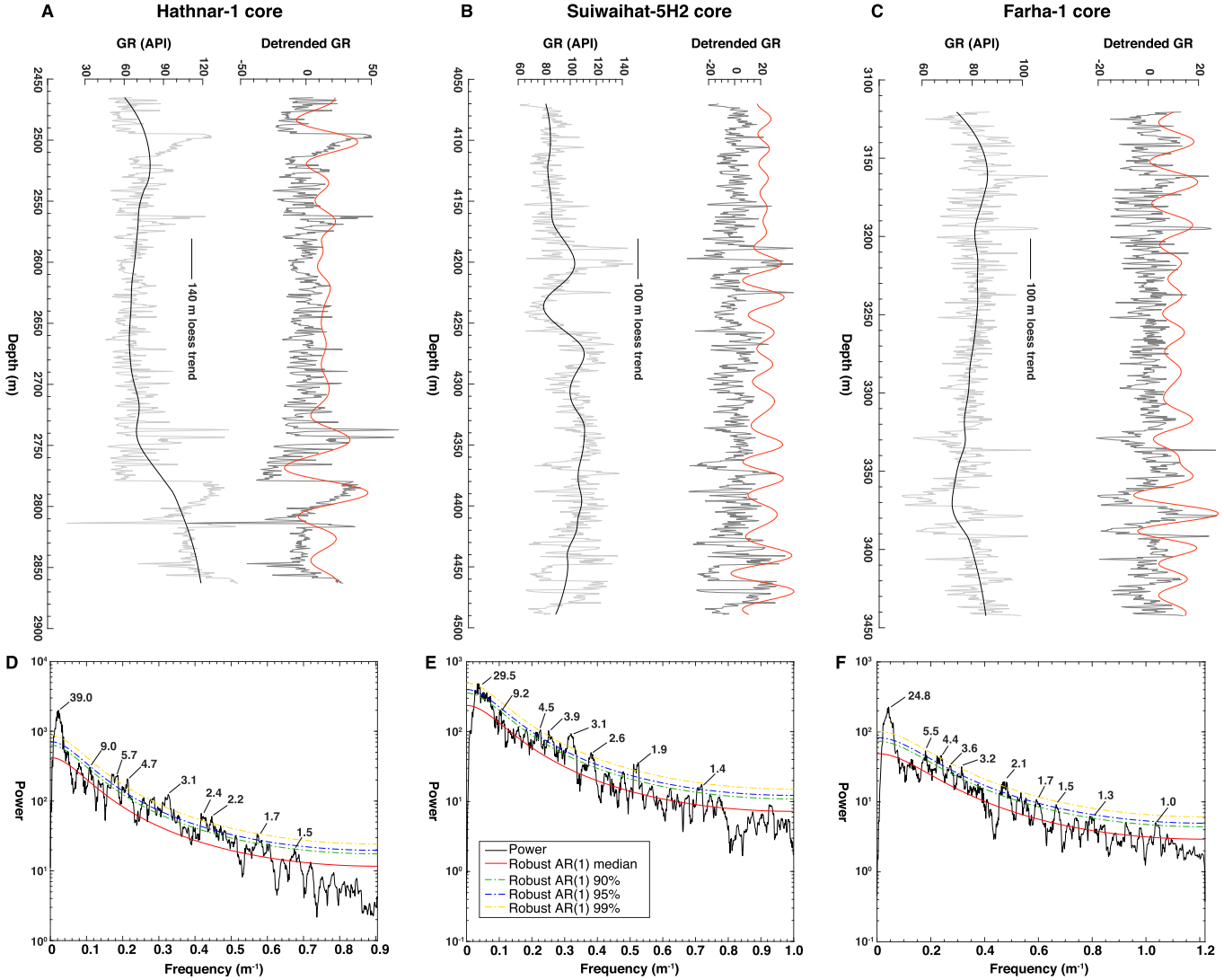

Fig. 4. GR series of the (A) Hathnar-1, (B) Suwaihat-5H2, and (C) Farha-1 cores. The light and dark grey lines and are the raw and detrended GR series, respectively. The black lines are the long-wavelength loess trends that are subtracted in detrending. The red lines are the Gaussian filter outputs of interpreted long eccentricity cycles. MTM power spectra of the (D) Hathnar-1, (E) Suwaihat-5H2, and (F) Farha-1 cores. Significant peaks are shown with the robust AR(1) red noise model, and the confidence levels of 90%, 95%, and 99%. The wavelengths of the significant peaks are shown in the power spectra. The unit of wavelength is meter. (For interpretation of the references to colour in this figure legend, the reader is referred to the web version of this article.)

example, the time span of the diamictites and the siliciclastic layers between the diamictites between 2460 m and 2240 m in the Hathnar-1 core will not be counted (Fig. 3). But this conservative approach is reasonable due to the lack of understanding of the astronomical forcing on the depositional process of diamictites as well as their sedimentation rates. Hence, the results should be taken as the minimum constraints on the duration of the Fiq Formation. GR data from the three cores were first interpolated to get evenly spaced series. Then, the long trend was removed using the locally estimated scatterplot smoothing (loess) regression (Fig. 4). The multi-taper method (MTM) spectral analysis (Thomson, 1982) was performed and the robust red noise was calculated using the model of Mann and Lees (1996). Peaks in the MTM power spectra are considered significant if they rise above the 95% confidence level of the robust red noise (Fig. 4). The wavelengths of the significant peaks were compared with the periodicities of Milankovitch cycles to get the average sedimentary accumulation rate (SAR) for the entire studied section (Table 1). Theoretical models that predict the periodicities of Milankovitch cycles in the Cryogenian are Laskar et al. (2004) and Waltham (2015). As a comparison, the statistical testing of the optimal SAR was also employed using the correlation coefficient (COCO) method of Li et al. (2018). In the COCO analysis, a range of possible SARs was surveyed from 2 cm/kyr to 20 cm/kyr, with an increment of 0.1 cm/kyr per step and 2000 Monte Carlo simulations. To explore the variation of SAR through the sections, the evolutionary correlation coefficient (eCOCO) analysis was also conducted (Li et al., 2018). The SAR range in the eCOCO analysis was also set to be 2–20 cm/kyr, with an increasing step of 0.1 cm/kyr and 2000 Monte Carlo simulations. The analytical software used is “Acycle” developed by Li et al. (2019b).

4. Results

4.1. Hathnar-1 core

The MTM spectral analysis yielded a suite of peaks that rise above the 95% confidence level of the robust red noise. The wavelengths of these significant peaks are 39.0, 9.0, 5.7, 4.7, 3.1, 2.4, 2.2, 1.7, and 1.5 m, respectively (Fig. 4D; Table 1). Comparison between the wavelengths of the significant peaks with the theoretical Milankovitch periodicities in Cryogenian time yields an average SAR for the studied segment of the Hathnar-1 core. Specifically, when the average SAR of 9.5 cm/kyr is applied, the 39.0 m peak corresponds to long eccentricity, the 9.0 m peak is close to short eccentricity, the 5.7 and 4.9 m peaks correlate with long obliquity, the 2.4, 2.2, and 1.7 m peaks are compatible with obliquity, and the 1.5 m peak corresponds to precession (Table 1). The GR series was filtered at the frequency of 1/39 m^{-1} that is interpreted to be long eccentricity. The filtered series reflects the cyclic pattern of the GR series (Fig. 4A). Using the average SAR and the stratigraphic thickness, the studied siliciclastic portion of the Fiq Formation in the Hathnar-1 core is ~4.2 Myr in duration.

The COCO analysis shows that the SARs of 8.6 cm/kyr and 9.9 cm/kyr have the highest correlation coefficient values (ρ) with the null hypothesis (H_0, no astronomical forcing) significance levels lower than 0.001 (Fig. 5). The eCOCO analysis supports an optimal SAR of 8–10 cm/kyr in 2860–2740 m and 2550–2465 m, consistent with the average SAR obtained in the MTM spectral analysis. However, the middle part of the GR series seems to be better fitted with a SAR of ~6 cm/kyr (Fig. 5). It is noticed that a SAR of 5.9 cm/kyr does show up as a peak in the COCO analysis, although its H_0 significance level is not as low as the other two SARs (Fig. 5). Constrained by the COCO and eCOCO results, the duration of the studied segment of the Fiq Formation in the Hathnar-1 core is ~5.5 Myr.

4.2. Suwaihat-5H2 core

A hierarchy of peaks above the 95% confidence level of the robust red noise was identified in the MTM power spectrum that is considered as significant. The wavelengths of these significant peaks are 29.5, 9.2, 4.5, 3.9, 3.1, 2.6, 1.9, and 1.4 m (Fig. 4E; Table 1). Compared with the theoretical periodicities of the Milankovitch cycles, an average SAR value of 7.3 cm/kyr was obtained for the Fig Formation in the Suwaihat-5H2 core. Using this SAR, the 29.5 m peak correlates with long eccentricity, the 9.2 m peak corresponds to short eccentricity, and the rest peaks fall into the wavelength ranges of long and short obliquities (Table 1). The filtered series at the long-eccentricity frequency of 1/29.5 m^{-1} mimics the general trend of the GR series (Fig. 4B). Based on the average SAR and the stratigraphic thickness, the Fiq Formation in the Suwaihat-5H2 core spans ~5.7 Myr.

The SAR of 7.3 cm/kyr has the highest ρ value, with the H_0

Table 1
Results of the MTM spectral analysis.

Hathnar-1 core (avg. SAR: 9.5 cm/kyr)			Suwaihat-5H2 core (avg. SAR: 7.3 cm/kyr)			Farha-1 core (avg. SAR: 6.1 cm/kyr)			Milankovitch cycles		
Frequency (m^{-1})	Wavelength (m)	Period (kyr)	Frequency (m^{-1})	Wavelength (m)	Period (kyr)	Frequency (m^{-1})	Wavelength (m)	Period (kyr)	Cycle	Period (kyr)	References
0.026	39.0	410.9	0.034	29.5	404.7	0.040	24.8	406.4	long eccentricity	405	Laskar et al. (2004)
0.111	9.0	94.8	0.109	9.2	125.5	0.181	5.5	90.5	short eccentricity	125; 95	Laskar et al. (2004)
0.177	5.7	59.5	0.225	4.5	61.0	0.229 0.274	4.4 3.6	71.6 59.8			
0.213	4.7	49.4	0.255	3.9	53.7	0.314	3.2	52.2	long obliquity	54	Hinnov (2013)
0.326	3.1	32.3	0.318 0.380	3.1 2.6	43.0 36.1	0.474	2.1	34.6			
0.423	2.4	24.9	0.520	1.9	26.4	0.593	1.7	27.6	obliquity	30.9 ± 4.6	Waltham (2015)
0.447	2.2	23.5				0.665	1.5	24.7			
0.574	1.7	18.3	0.717	1.4	19.1	0.796	1.3	20.6	precession	19.8 ± 1.9	Waltham (2015)
0.673	1.5	15.6				1.036	1.0	15.8		16.5 ± 1.4	

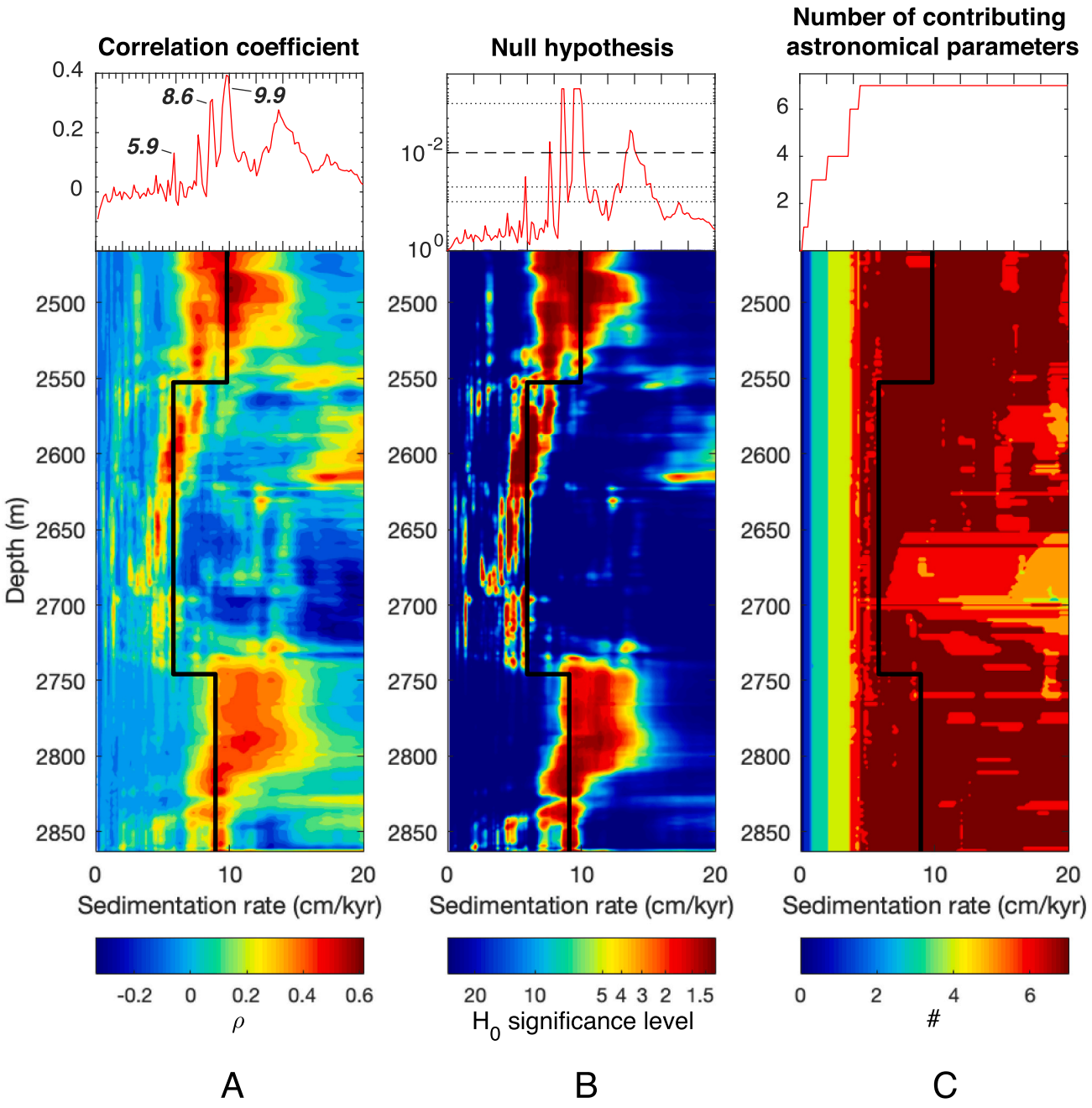

Fig. 5. The COCO and eCOCO results of the Hathnar-1 core. (A) Correlation coefficient (top) and evolutionary correlation coefficient (bottom). (B) Null hypothesis (H_0, no astronomical forcing; top) and evolutionary H_0 significance level (bottom). (C) The number of contributing astronomical parameters (top) and evolutionary number of contributing astronomical parameters (bottom). The optimal SARs are indicated with numbers. The unit of SAR is cm/kyr. The black lines delineate the changes in SAR through the stratigraphy. (For interpretation of the references to colour in this figure legend, the reader is referred to the web version of this article.)

significance level lower than 0.001 in the COCO analysis (Fig. 6). Besides, the SARs of 10.6 cm/kyr and 13.5 cm/kyr also bear high ρ values with low H_0 significance levels (Fig. 6). It turns out that these SARs control different parts of the GR series. Namely, the 7.3 cm/kyr rate best fits 4490–4310 m. This rate is similar to the result of the MTM spectral analysis. The SAR increases to ~10–13 cm/kyr between 4300 m and 4150 m. The upper part of the series is characterized by a SAR close to ~7.0 cm/kyr. According to the optimal rates suggested by the COCO and eCOCO results, the duration of the Fiq Formation in the Suwaihat-5H2 core is ~4.9 Myr.

4.3. Farha-1 core

In the MTM power spectrum, the peaks with wavelengths of 24.8, 5.5, 4.4, 3.6, 2.1, 1.7, 1.5, 1.3, and 1.0 m are above the 95% confidence level of the red noise (Fig. 4F). Significant peaks are assigned to Milankovitch cycles with an average SAR of 6.1 cm/kyr. Namely, the 24.8 m peak agrees with long eccentricity, the 5.5 m peak is close to short eccentricity, the 3.6 and 3.2 m peaks are consistent with long obliquity, the peaks with wavelengths between 2.1 and 1.3 m are obliquity, and the 1.0 m peak is precession. The series, after filtering at the long-eccentricity frequency of 1/24.8 m^{-1}, is in tune with the first-order variation of the GR series (Fig. 4C). With the obtained average SAR of 6.1 cm/kyr, A ~5.3 Myr duration was calculated for the 322-m Fiq

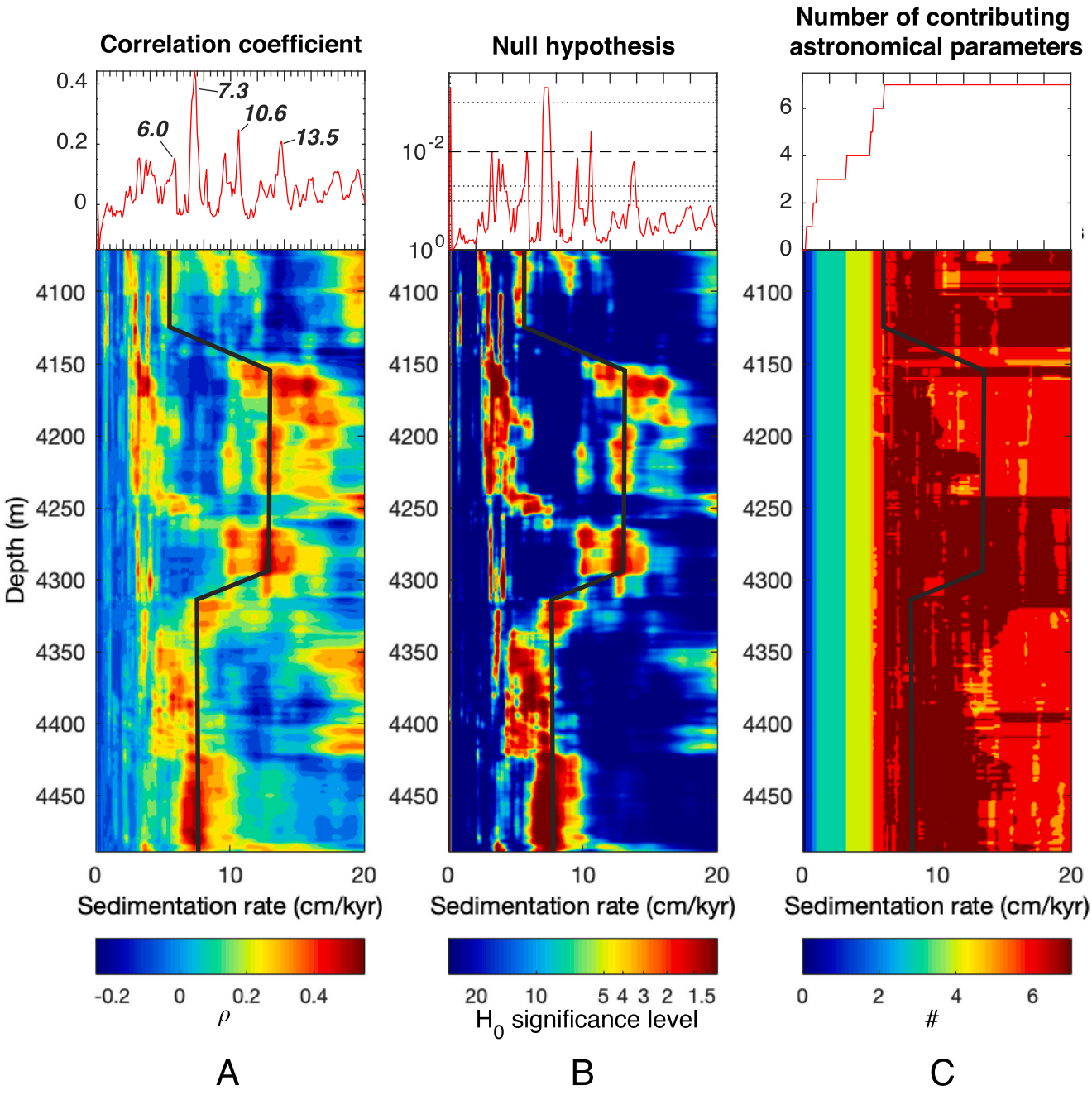

Fig. 6. The COCO and eCOCO results of the Suwaihat-5H2 core. (A) Correlation coefficient (top) and evolutionary correlation coefficient (bottom). (B) Null hypothesis (H_0, no astronomical forcing; top) and evolutionary H_0 significance level (bottom). (C) The number of contributing astronomical parameters (top) and evolutionary number of contributing astronomical parameters (bottom). The optimal SARs are indicated with numbers. The unit of SAR is cm/kyr. The black lines follow the changes in SAR through the stratigraphy. (For interpretation of the references to colour in this figure legend, the reader is referred to the web version of this article.)

Formation in the Farha-1 core.

Combing the results from the COCO and eCOCO analyses, the optimal SARs are 4.8 cm/kyr and 7.3 cm/kyr considering their high ρ values with low H_0 significance levels (Fig. 7). The SAR of 4.8 cm/kyr dominates in the bottom and upper parts and the rate of 7.3 cm/kyr controls the middle part of the series. The stratigraphic thickness of the Fiq Formation in the Farha-1 core can be translated to ~5.8 Myr in time when the optimal rates are applied.

5. Discussion

Astronomical forcing is thought to operate through geological time which modulates Earth's climate (Berger and Loutre, 1994; Hinnov, 2013, 2018). Based on a combination of the MTM, COCO, and eCOCO analyses, a complete suite of Milankovitch cycles has been identified, i.e. eccentricities, obliquities, and precessions (Table 1). The clear Milankovitch signals firmly support that the astronomically-forced climate cycles have influenced the depositional processes of the non-glacial units within the Fiq Formation. Specifically, the average SARs obtained from the MTM analyses show that Hathnar-1 core has a higher rate of 9.5 cm/kyr and the Farha-1 core has a lower rate of 6.1 cm/kyr (Table 1), which is consistent with the overall lithological observation that the Hathnar-1 core has thicker sandy layers while the Farha-1 core is totally composed of shaly and silty layers (Fig. 3). The eCOCO results show the SARs

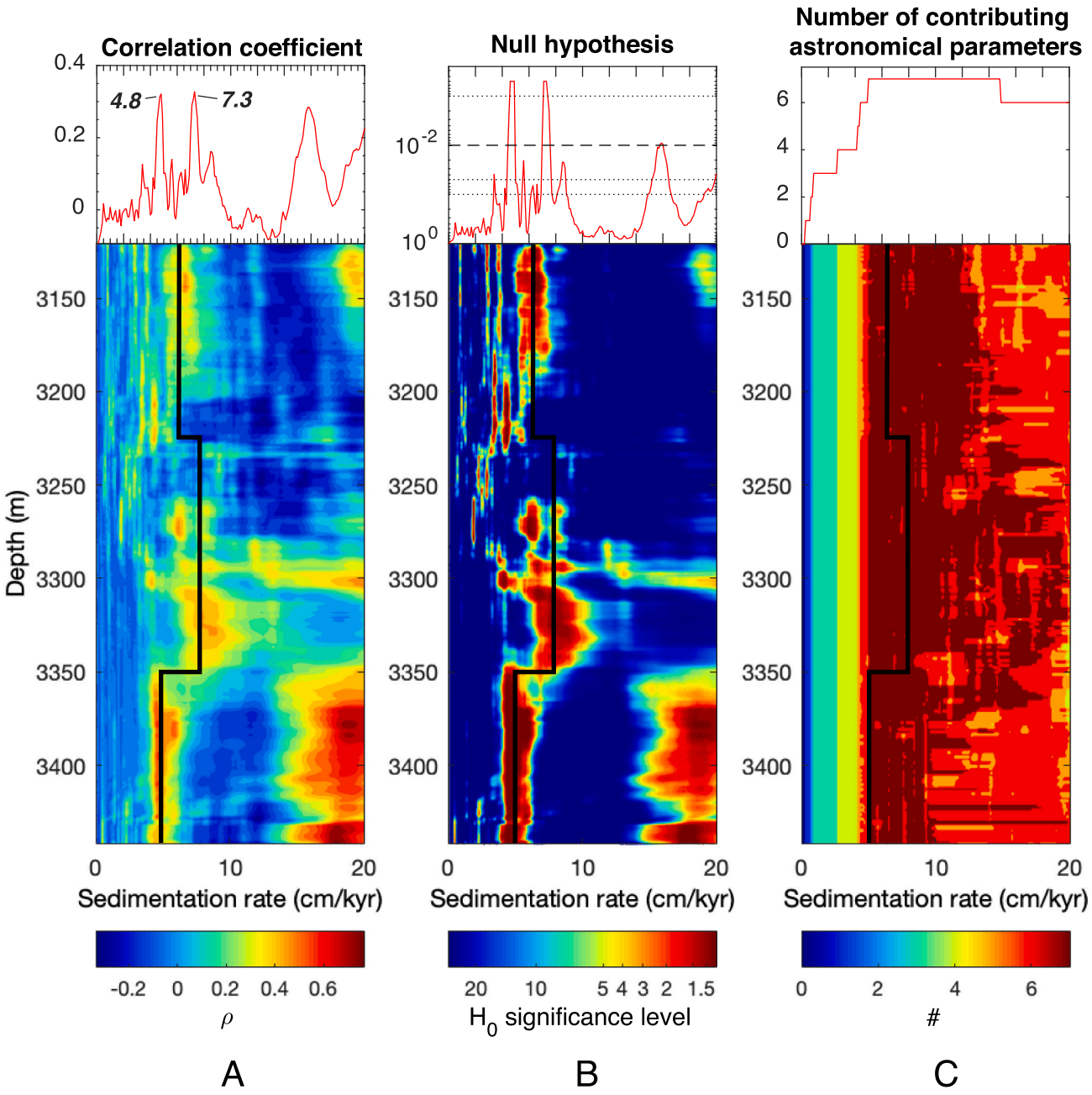

Fig. 7. The COCO and eCOCO results of the Farha-1 core. (A) Correlation coefficient (top) and evolutionary correlation coefficient (bottom). (B) Null hypothesis (H_0, no astronomical forcing; top) and evolutionary H_0 significance level (bottom). (C) The number of contributing astronomical parameters (top) and evolutionary number of contributing astronomical parameters (bottom). The optimal SARs are indicated with numbers. The unit of SAR is cm/kyr. The black lines show the changes in SAR through the stratigraphy. (For interpretation of the references to colour in this figure legend, the reader is referred to the web version of this article.)

variations through the cores and suggest that different SARs dominate different lithological layers. For instance, in the Hathnar-1 core, the shaly and silty layers in the bottom are characterized by a SAR of ~8–10 cm/kyr. The overlying sandy layers have a slightly lower rate of ~6 cm, which increases to 8–10 cm/kyr again in the upper sandy layers below the diamictites (Figs. 3 and 5). Although the decrease of SAR from 8–10 cm/kyr to 6 cm/kyr at 2740 m in the Hathnar-1 core seems to be at odds with the lithological change, these rates are within the reasonable range for these lithologies. The SARs are likely controlled by local source variations due to the rift basin depositional environment. Within the sandstone layers in the upper part of the core, SARs also show an increase, supporting the local influences on deposition. Varying SARs are also observed in the other two cores. Specifically, in the Suwaihat-5H2 core, a lower SAR of 7.3 cm/kyr corresponds to the shales and siltstones in the lower part, a higher SAR of 10–13 cm/kyr relates to the upper part where sandy layers predominate, and a return back to a lower SAR at the very top when silty layers appear again (Figs. 3 and 6). It should be noticed that in the 4250–4100 m segment of the Suwaihat-5H2 core, a SAR of 4.0 cm/kyr could also yield a high ρ value with a low H_0 value (Fig. 6). However, this high ρ value is achieved by only matching 4 targeted Milankovitch cycles (Fig. 6c) while the preferred SAR of 10–13 cm/kyr has taken all 7 targeted Milankovitch cycles into consideration. Therefore, this 4.0 cm/kyr is not optimal and it also contradicts with the lithological indication of the SAR, because this interval is made mainly of sandstones and thus should have a higher instead of lower SAR (Figs. 3 and 6). In the Farha-1 core, there are no

dominant sandy layers but there exist alternating shales and siltstones (Fig. 3). Therefore, the SARs of the Farha-1 core do not shift as significantly as the Hathnar-1 and Suwaihat-5H2 cores, but instead, show more gradual changes between 4.8 cm/kyr and 7.3 cm/kyr (Fig. 7), and are generally slower with respect to the other cores.

The encoding mechanism of the Milankovitch cycles in the Fiq Formation is likely a combination of both the changes in the terrigenous input and fluctuations in sea level, which are modulated astronomically and can be reflected by the variations in GR values. The lithology of the Fiq Formation indicates a "soft" Snowball Earth scenario (Allen and Etienne, 2008). The hydrological cycle during the Snowball Earth events should not be completely shut down (Allen, 2007; Rieu et al., 2007), and should be sensitive to astronomical forcing (Benn et al., 2015; Mitchell et al., 2021b), at least in low-latitude areas where Oman was located (Kempf et al., 2000; Kilner et al., 2005). During the warm and humid periods, chemical weathering would enhance the production of clay minerals, which are efficiently transported by large runoff fluxes to the ocean, leading to higher GR values. On the contrary, during the cold and dry periods, physical weathering regime dominates and the clay production would be reduced due to the weakened hydrological cycle, making GR values lower. Besides, under cold and dry conditions, the changes in terrigenous supply would be overshadowed by sea level fluctuations (Van der Zwan, 2002). Hence, the varying sea level could subtly oscillate the depositional environment, which leads to the change in grain size and clastic concentration that are reflected by GR values.

The average SARs estimated from the MTM spectral analysis is similar but not as detailed as the optimal SARs obtained from the integrated COCO-eCOCO analysis, thus, resulting in different estimates on the duration of the Fiq Formation. The integrated COCO-eCOCO analysis is apparently a more reasonable approach since it takes the lithological variations into consideration. Because of this, the duration of the non-glacial units of the Fiq Formation should be ~5.5 Myr in the Hathnar-1 core, ~4.9 Myr in the Suwaihat-5H2 core, and ~5.8 Myr in the Farha-1 core. It needs to be pointed out that these duration estimates can only be considered conservative. The duration of the glaciogenic units, i.e. diamictites, are difficult to be evaluated due to the episodic nature of the glaciogenic deposition. Thus, the Fiq Formation lasts at least for ~6 million years.

If ~635 Ma is used as the termination age of the Marinoan glaciation (Condon et al., 2005; Hoffman et al., 2017), based on the results of this study, its onset age should be no younger than ~641 Ma. This estimate is in consistent with the minimum onset age constraint from the Ghaub Formation in Namibia, which is 639.3 ± 0.3 Ma (U-Pb TIMS zircon age, Prave et al., 2016; Fig. 1B). The maximum onset age of the Marinoan glaciation has also been suggested by many workers, ranging from 657 Ma to 651 Ma (Fig. 1B; Zhang et al., 2008; Lan et al., 2015; Nelson et al., 2020; Rooney et al., 2020). Since it could be difficult to find an ash bed or a black shale layer immediately below the Marinoan diamictite, how close these maximum ages to the true onset age of the glaciation largely depends on the stratigraphic distance as well as the sedimentation rate. Other complexities could result from the uncertainties of the radiometric ages especially the Re-Os ages, and the basal erosion by the glaciation. However, Bao et al. (2018) used a different approach to tackle this problem. Bao et al. (2018) conducted a cyclostratigraphic study to directly estimate the timespan between Sturtian and Marinoan glaciations. By counting the Milankovitch cycles preserved in the Datangpo Formation in South China, Bao et al. (2018) suggested that the Sturtian and Marinoan glaciations were separated by ~10 million years. Bao et al. (2018) also claimed that there is no significant depositional gap recognized within the Datangpo Formation and the stratigraphic transition to the Nantuo diamictites is gradational, thus, no apparent glacial erosion effect. If this is true, the Datangpo Formation provides the most complete record between the two Snowball Earth events. Taken ~660 Ma as the termination age of the Sturtian glaciation (Hoffman et al., 2017) as well as Bao et al. (2018)'s constraint, the Marinoan glaciation was initiated at ~650 Ma. This ~650 Ma estimate is in good agreement with the maximum constraints from the radiometric ages obtained from South China and Laurentia (Fig. 1B; Zhang et al., 2008; Lan et al., 2015; Nelson et al., 2020; Rooney et al., 2020). However, Kendall et al. (2006), by dating the Tindelpina Shale in South Australia, proposed that the onset age of the Marinoan glaciation should be younger than 643.0 ± 2.4 Ma. The uncertainty of this Re-Os age is relatively large, making it less powerful to pinpoint the age of the Marinoan glaciation. Besides, the robustness of this 643.0 ± 2.4 Ma age is challenged by Rooney et al. (2014), stating that the analytical error and stratigraphic correlation in Kendall et al. (2006)'s work are problematic. Given all complexities regarding this Re-Os age (Kendall et al., 2006), and considering the cyclostratigraphic work of Bao et al. (2018) and this study, the onset age of the Marinoan glaciation should be 650–641 Ma, and likely closer to 650 Ma.

The chronology of the Marinoan glaciation is of great significance for understanding the nature of this event. Various models have been proposed to explain the initiation of Snowball Earth events (e.g., Schrag et al., 2002; Goddéris et al., 2003; Cox et al., 2016; Macdonald and Wordsworth, 2017). However, there are many differences between the Sturtian and Marinoan glaciations that still lack satisfying explanations (Hoffman et al., 2017). First and foremost is the apparent difference in their durations. The Sturtian glaciation is 57-million-year long, from ~717 Ma to ~660 Ma (Hoffman et al., 2017). However, based on the new constraint of this study, the Marinoan glaciation lasts only 6–15 million years, much briefer compared with its predecessor. Another important aspect is that the two Snowball Earth events are temporally separated by merely 10–17 million years. No matter what mechanism is invoked as the trigger for the Snowball Earth events, it has to explain the fast drawdown of CO_2 from the atmosphere in order to initiate the Marinoan glaciation that is immediately after the Sturtian glaciation, as well as the fast buildup of CO_2 during the Marinoan glaciation to overcome the ice-albedo feedback and eventually lead to the deglaciation. The results of this study provide critical time constraints for the geological and numerical models related to the Cryogenian Snowball Earth events.

6. Conclusions

Based on the cyclostratigraphic study on the three drilled sections of the Cryogenian Fiq Formation in Oman, Milankovitch cycles that are encoded in the variations of the GR values have been successfully identified. The obtained SARs from the MTM spectral analysis and the integrated COCO-eCOCO analysis yield a conservative duration for the Fiq Formation, which is no less than ~6 Myr. Coupled with the available U-Pb and Re-Os ages, the onset age of the Marinoan glaciation should be between 650 Ma and 641 Ma, supporting that the Marinoan glaciation is much briefer than the Sturtian glaciation. These new results further constrain the timespans of the Marinoan glaciation and the interglacial period between the two Cryogenian Snowball Earth events, and provide critical time scales for the geological and numerical models that explore questions such as how the Marinoan glaciation was initiated quite shortly after its predecessor, why the Marinoan glaciation was a much short-lived Snowball Earth event, and how the extreme climate changes were connected with the changes in global carbon cycle and biosphere in Cryogenian time.

Declaration of Competing Interest

The authors declare that they have no known competing financial interests or personal relationships that could have appeared to influence the work reported in this paper.

Acknowledgements

Zheng Gong was supported by the Yale Graduate School Fellowship. I thank Jikai Ding for helpful discussion, and two anonymous reviewers

for constructive suggestions.

Appendix A. Supplementary data

Supplementary data to this article can be found online at https://doi.org/10.1016/j.gloplacha.2021.103584.

References

Allen, P.A., 2007. The Huqf Supergroup of Oman: basin development and context for Neoproterozoic glaciation. Earth Sci. Rev. 84 (3–4), 139–185.

Allen, P.A., Etienne, J.L., 2008. Sedimentary challenge to snowball Earth. Nat. Geosci. 1 (12), 817–825.

Allen, P.A., Leather, J., Brasier, M.D., Rieu, R., McCarron, M., le Guerroué, E., Cozzi, A., 2011. The Abu Mahara Group (Ghubrah and Fiq formations), Jabal Akhdar, Oman. Geol. Soc. Lond. Mem. 36 (1), 251–262.

Bao, X., Zhang, S., Jiang, G., Wu, H., Li, H., Wang, X., Yang, T., 2018. Cyclostratigraphic constraints on the duration of the Datangpo Formation and the onset age of the Nantuo (Marinoan) glaciation in South China. Earth Planet. Sci. Lett. 483, 52–63.

Benn, D.I., Le Hir, G., Bao, H., Donnadieu, Y., Dumas, C., Fleming, E.J., Fairchild, I.J., 2015. Orbitally forced ice sheet fluctuations during the Marinoan Snowball Earth glaciation. Nature Geoscience 8 (9), 704–707.Chicago.

Berger, A., Loutre, M.F., 1994. Astronomical forcing through geological time. In: De Boer, P.L., Smith, D.G. (Eds.), Orbital forcing and cyclic sequences, 19. Blackwell Scientific Publications Oxford, pp. 15–24.

Bowring, S.A., Grotzinger, J.P., Condon, D.J., Ramezani, J., Newall, M.J., Allen, P.A., 2007. Geochronologic constraints on the chronostratigraphic framework of the Neoproterozoic Huqf Supergroup, Sultanate of Oman. Am. J. Sci. 307 (10), 1097–1145.

Brasier, M., McCarron, G., Tucker, R., Leather, J., Allen, P., Shields, G., 2000. New U-Pb zircon dates for the Neoproterozoic Ghubrah glaciation and for the top of the Huqf Supergroup, Oman. Geology 28 (2), 175–178.

Cantine, M., Bergmann, K., Rooney, A.D., Linnemann, U., Hofmann, M., Albert, R., Gerdes, A., 2019. Geochronologic constraints on the Shuram excursion in Oman. In: AGU Fall Meeting Abstracts, 2019. PP51E-1409.

Cheng, D., Zhang, S., Zhang, Z., Zhou, C., Wang, H., Yuan, X., Chen, X., 2020. An astronomically calibrated stratigraphy of the Mesoproterozoic Hongshuizhuang formation, North China: implications for pre-Phanerozoic changes in Milankovitch orbital parameters. J. Asian Earth Sci. 199, 104408.

Condon, D., Zhu, M., Bowring, S., Wang, W., Yang, A., Jin, Y., 2005. U-Pb ages from the neoproterozoic doushantuo formation, China. Science 308 (5718), 95–98.

Cox, G.M., Halverson, G.P., Stevenson, R.K., Vokaty, M., Poirier, A., Kunzmann, M., Macdonald, F.A., 2016. Continental flood basalt weathering as a trigger for Neoproterozoic Snowball Earth. Earth Planet. Sci. Lett. 446, 89–99.

Cramer, B.D., Jarvis, I., 2020. Carbon isotope stratigraphy. In: Geologic Time Scale 2020. Elsevier, pp. 309–343.

Fairchild, I.J., Bonnand, P., Davies, T., Fleming, E.J., Grassineau, N., Halverson, G.P., Stevenson, C.T., 2016. The late Cryogenian warm interval, NE Svalbard: chemostratigraphy and genesis. Precambrian Res. 281, 128–154.

Forbes, G.A., Jansen, H.S., Schreurs, J., 2010. Lexicon of Oman: Subsurface Stratigraphy: Reference Guide to the Stratigraphy of Oman's Hydrocarbon Basins (Gulf PetroLink).

Goddéris, Y., Donnadieu, Y., Nédélec, A., Dupré, B., Dessert, C., Grard, A., François, L.M., 2003. The Sturtian 'snowball' glaciation: fire and ice. Earth Planet. Sci. Lett. 211 (1–2), 1–12.

Gong, Z., Li, M., 2020. Astrochronology of the Ediacaran Shuram carbon isotope excursion, Oman. Earth Planet. Sci. Lett. 547, 116462.

Gong, Z., Kodama, K.P., Li, Y.X., 2017. Rock magnetic cyclostratigraphy of the Doushantuo Formation, South China and its implications for the duration of the Shuram carbon isotope excursion. Precambrian Res. 289, 62–74.

Gong, Z., Kodama, K.P., Li, Y.X., 2019. Paleomagnetism and rock magnetic cyclostratigraphy of the Ediacaran Doushantuo Formation, South China: Constraints on the remagnetization mechanism and the encoding process of Milankovitch cycles. Palaeogeogr. Palaeoclimatol. Palaeoecol. 528, 232–246.

Gorin, G.E., Racz, L.G., Walter, M.R., 1982. Late Precambrian-Cambrian sediments of Huqf Group, Sultanate of Oman. AAPG Bull. 66 (12), 2609–2627.

Hansman, R.J., Ring, U., Thomson, S.N., den Brok, B., Stübner, K., 2017. Late Eocene uplift of the Al Hajar Mountains, Oman, supported by stratigraphy and low-temperature thermochronology. Tectonics 36 (12), 3081–3109.

Hinnov, L.A., 2013. Cyclostratigraphy and its revolutionizing applications in the earth and planetary sciences. GSA Bull. 125 (11−12), 1703–1734.

Hinnov, L.A., 2018. Cyclostratigraphy and astrochronology in 2018. In: Stratigraphy & Timescales, 3. Academic Press, pp. 1–80.

Hoffman, P.F., Kaufman, A.J., Halverson, G.P., Schrag, D.P., 1998. A Neoproterozoic snowball earth. Science 281 (5381), 1342–1346.

Hoffman, P.F., Abbot, D.S., Ashkenazy, Y., Benn, D.I., Brocks, J.J., Cohen, P.A., Warren, S.G., 2017. Snowball Earth climate dynamics and Cryogenian geology-geobiology. Sci. Adv. 3 (11), e1600983.

Kempf, O., Kellerhals, P., Lowrie, W., Matter, A., 2000. Paleomagnetic directions in late Precambrian glaciomarine sediments of the Mirbat Sandstone Formation, Oman. Earth Planet. Sci. Lett. 175 (3–4), 181–190.

Kendall, B., Creaser, R.A., Selby, D., 2006. Re-Os geochronology of postglacial black shales in Australia: Constraints on the timing of "Sturtian" glaciation. Geology 34 (9), 729–732.

Kilner, B., Niocaill, C., Brasier, M., 2005. Low-latitude glaciation in the Neoproterozoic of Oman. Geology 33 (5), 413–416.

Kirschvink, J.L., 1992. Late Proterozoic low-latitude global glaciation: the snowball Earth. In: Schopf, J.W., Klein, C., Des Maris, D. (Eds.), The Proterozoic Biosphere: A Multidisciplinary Study. Cambridge University Press, pp. 51–52.

Kodama, K.P., Hinnov, L.A., 2014. Rock Magnetic Cyclostratigraphy. John Wiley & Sons.

Lan, Z., Li, X.H., Zhang, Q., Li, Q.L., 2015. Global synchronous initiation of the 2nd episode of Sturtian glaciation: SIMS zircon U-Pb and O isotope evidence from the Jiangkou Group, South China. Precambrian Res. 267, 28–38.

Lantink, M.L., Davies, J.H., Mason, P.R., Schaltegger, U., Hilgen, F.J., 2019. Climate control on banded iron formations linked to orbital eccentricity. Nat. Geosci. 12 (5), 369–374.

Laskar, J., Robutel, P., Joutel, F., Gastineau, M., Correia, A.C.M., Levrard, B., 2004. A long-term numerical solution for the insolation quantities of the Earth. Astron. Astrophys. 428 (1), 261–285.

Leather, J., Allen, P.A., Brasier, M.D., Cozzi, A., 2002. Neoproterozoic snowball Earth under scrutiny: evidence from the Fiq glaciation of Oman. Geology 30 (10), 891–894.

Lewis, J.P., Weaver, A.J., Eby, M., 2007. Snowball versus slushball Earth: dynamic versus nondynamic sea ice? J. Geophys. Res. Oceans 112, C11014.

Li, M., Kump, L.R., Hinnov, L.A., Mann, M.E., 2018. Tracking variable sedimentation rates and astronomical forcing in Phanerozoic paleoclimate proxy series with evolutionary correlation coefficients and hypothesis testing. Earth Planet. Sci. Lett. 501, 165–179.

Li, M., Huang, C., Ogg, J., Zhang, Y., Hinnov, L., Wu, H., Zou, Z., 2019a. Paleoclimate proxies for cyclostratigraphy: comparative analysis using a lower Triassic marine section in South China. Earth Sci. Rev. 189, 125–146.

Li, M., Hinnov, L., Kump, L., 2019b. Acycle: time-series analysis software for paleoclimate research and education. Comput. Geosci. 127, 12–22.

Lyu, D., Deng, Y., Wang, H., Zhang, F., Ren, R., Gao, Z., Canfield, D.E., 2021. Using cyclostratigraphic evidence to define the unconformity caused by the Mesoproterozoic Qinyu Uplift in the North China Craton. J. Asian Earth Sci. 206, 104608.

Macdonald, F.A., Wordsworth, R., 2017. Initiation of Snowball Earth with volcanic sulfur aerosol emissions. Geophys. Res. Lett. 44 (4), 1938–1946.

Mann, M.E., Lees, J.M., 1996. Robust estimation of background noise and signal detection in climatic time series. Clim. Chang. 33 (3), 409–445.

Mei, M.X., Tucker, M.E., 2013. Milankovitch-driven cycles in the Precambrian of China: the Wumishan formation. J. Palaeogeogr. 2 (4), 369–389.

Minguez, D., Kodama, K.P., 2017. Rock magnetic chronostratigraphy of the Shuram carbon isotope excursion: wonoka formation, Australia. Geology 45 (6), 567–570.

Minguez, D., Kodama, K.P., Hillhouse, J.W., 2015. Paleomagnetic and cyclostratigraphic constraints on the synchroneity and duration of the Shuram carbon isotope excursion, Johnnie Formation, Death Valley Region, CA. Precambrian Res. 266, 395–408.

Mitchell, R.N., Kirscher, U., Kunzmann, M., Liu, Y., Cox, G.M., 2021a. Gulf of Nuna: astrochronologic correlation of a Mesoproterozoic oceanic euxinic event. Geology 49 (1), 25–29.

Mitchell, R.N., Gernon, T.M., Cox, G.M., Nordsvan, A.R., Kirscher, U., Xuan, C., He, X., 2021b. Orbital forcing of ice sheets during snowball Earth. Nature Communications 12 (1), 1–9.

Nelson, L.L., Smith, E.F., Hodgin, E.B., Crowley, J.L., Schmitz, M.D., Macdonald, F.A., 2020. Geochronological constraints on Neoproterozoic rifting and onset of the Marinoan glaciation from the Kingston Peak Formation in Death Valley, California (USA). Geology 48 (11), 1083–1087.

Prave, A.R., Condon, D.J., Hoffmann, K.H., Tapster, S., Fallick, A.E., 2016. Duration and nature of the end-Cryogenian (Marinoan) glaciation. Geology 44 (8), 631–634.

Rieu, R., Allen, P.A., Plötze, M., Pettke, T., 2007. Climatic cycles during a Neoproterozoic "snowball" glacial epoch. Geology 35 (4), 299–302.

Rodrigues, P.D.O.C., Hinnov, L.A., Franco, D.R., 2019. A new appraisal of depositional cyclicity in the Neoarchean-Paleoproterozoic Dales Gorge Member (Brockman Iron Formation, Hamersley Basin, Australia). Precambrian Res. 328, 27–47.

Rooney, A.D., Macdonald, F.A., Strauss, J.V., Dudás, F.Ö., Hallmann, C., Selby, D., 2014. Re-Os geochronology and coupled Os-Sr isotope constraints on the Sturtian snowball Earth. Proc. Natl. Acad. Sci. 111 (1), 51–56.

Rooney, A.D., Yang, C., Condon, D.J., Zhu, M., Macdonald, F.A., 2020. U-Pb and Re-Os geochronology tracks stratigraphic condensation in the Sturtian snowball Earth aftermath. Geology 48 (6), 625–629.

Schrag, D.P., Berner, R.A., Hoffman, P.F., Halverson, G.P., 2002. On the initiation of a snowball Earth. Geochem. Geophys. Geosyst. 3 (6), 1–21.

Shields-Zhou, G.A., Porter, S., Halverson, G.P., 2016. A new rock-based definition for the Cryogenian Period (circa 720-635 Ma). Episodes 39 (1), 3–8.

Sui, Y., Huang, C., Zhang, R., Wang, Z., Ogg, J., Kemp, D.B., 2018. Astronomical time scale for the lower Doushantuo Formation of early Ediacaran, South China. Sci. Bull. 63 (22), 1485–1494.

Sui, Y., Huang, C., Zhang, R., Wang, Z., Ogg, J., 2019. Astronomical time scale for the middle-upper Doushantuo Formation of Ediacaran in South China: implications for the duration of the Shuram/Wonoka negative $\delta^{13}C$ excursion. Palaeogeogr. Palaeoclimatol. Palaeoecol. 532, 109273.

Thomson, D.J., 1982. Spectrum estimation and harmonic analysis. Proc. IEEE 70 (9), 1055–1096.

Van der Zwan, C.J., 2002. The impact of Milankovitch-scale climatic forcing on sediment supply. Sediment. Geol. 147 (3–4), 271–294.

Waltham, D., 2015. Milankovitch period uncertainties and their impact on cyclostratigraphy. J. Sediment. Res. 85 (8), 990–998.

Yang, J., Peltier, W.R., Hu, Y., 2012. The initiation of modern soft and hard Snowball Earth climates in CCSM4. Clim. Past 8 (3), 907–918.
Zhang, S., Jiang, G., Han, Y., 2008. The age of the Nantuo Formation and Nantuo glaciation in South China. Terra Nova 20 (4), 289–294.
Zhang, S., Evans, D.A., Li, H., Wu, H., Jiang, G., Dong, J., Yang, T., 2013. Paleomagnetism of the late Cryogenian Nantuo Formation and paleogeographic implications for the South China Block. J. Asian Earth Sci. 72, 164–177.
Zhang, S., Wang, X., Hammarlund, E.U., Wang, H., Costa, M.M., Bjerrum, C.J., Canfield, D.E., 2015. Orbital forcing of climate 1.4 billion years ago. Proc. Natl. Acad. Sci. 112 (12), E1406–E1413.